J. Am. Soc. Mass Spectrom. (2017) 28:1166–1174
DOI: 10.1007/s13361-016-1570-2

FOCUS: HONORING R. G. COOKS' ELECTION TO THE NATIONAL ACADEMY OF SCIENCES: RESEARCH ARTICLE

Detection of Metastatic Breast and Thyroid Cancer in Lymph Nodes by Desorption Electrospray Ionization Mass Spectrometry Imaging

Jialing Zhang,[1] Clara L. Feider,[1] Chandandeep Nagi,[2] Wendong Yu,[2] Stacey A. Carter,[3] James Suliburk,[3] Hop S. Tran Cao,[3] Livia S. Eberlin[1]

[1]Department of Chemistry, The University of Texas at Austin, Austin, TX 78712, USA
[2]Department of Pathology and Immunology, Baylor College of Medicine, Houston, TX 77030, USA
[3]Department of Surgery, Baylor College of Medicine, Houston, TX 77030, USA

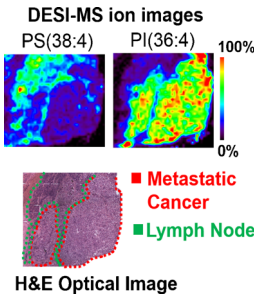

Abstract. Ambient ionization mass spectrometry has been widely applied to image lipids and metabolites in primary cancer tissues with the purpose of detecting and understanding metabolic changes associated with cancer development and progression. Here, we report the use of desorption electrospray ionization mass spectrometry (DESI-MS) to image metastatic breast and thyroid cancer in human lymph node tissues. Our results show clear alterations in lipid and metabolite distributions detected in the mass spectra profiles from 42 samples of metastatic thyroid tumors, metastatic breast tumors, and normal lymph node tissues. 2D DESI-MS ion images of selected molecular species allowed discrimination and visualization of specific histologic features within tissue sections, including regions of metastatic cancer, adjacent normal lymph node, and fibrosis or adipose tissues, which strongly correlated with pathologic findings. In thyroid cancer metastasis, increased relative abundances of ceramides and glycerophosphoinisitols were observed. In breast cancer metastasis, increased relative abundances of various fatty acids and specific glycerophospholipids were seen. Trends in the alterations in fatty acyl chain composition of lipid species were also observed through detailed mass spectra evaluation and chemical identification of molecular species. The results obtained demonstrate DESI-MSI as a potential clinical tool for the detection of breast and thyroid cancer metastasis in lymph nodes, although further validation is needed.

Keywords: Mass spectrometry imaging, Metastatic cancer, Cancer staging, Lipid profiles, Ambient mass spectrometry

Received: 4 November 2016/Revised: 24 November 2016/Accepted: 27 November 2016/Published Online: 28 February 2017

Introduction

Mass spectrometry imaging (MSI) has emerged as a powerful technology for biomedical applications, as it allows chemical characterization and visualization of the spatial distribution of molecules in a variety of biological tissues [1]. In particular, cancer tissue diagnosis using ambient ionization MSI approaches has been explored by several research groups [2]. For instance, DESI-MSI, the most commonly used ambient ionization MS technique, has been employed to analyze many primary human cancer tissues, including brain [3], prostate [4], gastric [5], kidney [6], and breast [7, 8]. Other ambient ionization MSI techniques such as laser ablation electrospray ionization mass spectrometry (LAESI-MS) [9], rapid evaporative ionization mass spectrometry (REIMS) [10], and nano-DESI [11] have been used to investigate the molecular signatures of biological samples and for cancer diagnosis [2, 12, 13]. Notably, ambient ionization MS techniques bring the advantages of speed and simplicity for molecular evaluation of clinical specimens, and features that are highly attractive for real time diagnosis of tissue specimens in clinical practice.

Electronic supplementary material The online version of this article (doi:10.1007/s13361-016-1570-2) contains supplementary material, which is available to authorized users.

Correspondence to: Livia Eberlin; *e-mail:* liviase@utexas.edu

Cancer staging routinely involves evaluation of regional lymph nodes for presence of metastatic cancer cells. The TNM system is widely used for cancer staging, in which "N" refers to the status of nearby lymph nodes to which the primary tumor has metastasized. The nodal status (value of "N") plays an important role in determining cancer stage and subsequent treatments. Intraoperative lymph node analysis is commonly performed by histopathologic evaluation of frozen sections or touch imprint cytology. In breast cancer surgery, for example, sentinel lymph node dissection has become a standard technique for staging the axilla and determining the extent of surgical resection. In a study performed on 13,062 breast cancer patients, intraoperative frozen section analysis by histopathologic evaluation allowed metastatic breast cancer detection with a mean sensitivity and specificity of 73% and 100%, respectively [14]. Besides traditional histopathology, other molecular and optical imaging techniques have been explored to provide more accurate detection and staging of cancer in lymph node tissues, including one-step nucleic acid amplification (OSNA) [15], radio-lympho-scintigraphy [16], Raman spectrometry [17], and positron emission tomography (PET) [18, 19]. Matrix assisted laser desorption ionization MSI has been successfully used to identify lymph node metastasis in colorectal, colon, prostate, and breast cancers based on protein detection [20–23]. More recently, DESI-MSI was used to identify lymph node metastasis from esophageal adenocarcinoma and gastric cancer. In gastric cancer, metabolic profile of the metastatic cancer within lymph nodes was found to be similar to that of the primary tumor site when analyzed by DESI-MSI [24]. In esophageal adenocarcinoma, DESI-MSI allowed objective identification of lymph node metastasis based on its primary tumor lipid profile, with an accuracy of 97.7% in comparison to histopathologic evaluation [25].

Here, we investigated the usefulness of DESI-MSI for detecting and visualizing metastatic breast and thyroid cancers in lymph node samples. Identification of metabolites, fatty acids (FA), glycerophospholipids (GP), sphingolipids (SL), and glycolipids (GL) was performed to molecularly characterize metastatic tissues within lymph nodes and normal lymph nodes. Various subtypes of complex lipids, such as ceramides (Cer), diacylglycerolipids (DG), triacylglycerolipids (TG), glycerophosphoglycerols (PG), glycerophosphoethanolamines (PE), cardiolipins (CL), glycerophosphoserines (PS), and glycerophosphoinositols (PI) were identified. Trends in the changes of molecular patterns, including variations of degrees of unsaturation of lipid acyl chains were observed in the mass spectra profiles obtained. 2D mapping of the molecules within the tissue sections showed that DESI-MSI allows clear discrimination of cancer metastasis from normal lymphatic and supportive tissue, thus proving evidence that DESI-MSI can be used for lymph node staging in breast and thyroid cancer.

Experimental

Tissue Samples

Banked frozen human tissue samples, including normal human lymph nodes (n = 18), lymph node with metastatic breast cancer (n = 16), and lymph node with metastatic papillary thyroid cancer (n = 8) were obtained from Cooperative Human Tissue Network (CHTN) under approved IRB protocol. Samples were stored in a –80 °C freezer until sectioned. Tissue samples were sectioned at 16 µm thick sections using a CryoStar NX50 cryostat (Thermo Scientific, San Jose, CA, USA). After sectioning, the glass slides were stored in a –80 °C freezer. Prior to MSI, the glass slides were dried for ~15 min.

DESI-MS Imaging

A 2D Omni Spray (Prosolia Inc., Indianapolis, IN, USA) was used for tissue imaging with a spatial resolution of 150 µm. DESI-MSI was performed in the negative ion mode from *m/z* 100 to 1500, using a hybrid LTQ-Orbitrap Elite mass spectrometer (Thermo Scientific). Mass spectra were acquired in centroid mode. The histologically compatible solvent system dimethylformamide:acetonitrile 1:1 was used for analysis.

Tissue Staining

The same tissue sections analyzed by DESI-MSI were stained using standard H&E staining protocol. Pathologic evaluation was performed using light microscopy by two dedicated surgical pathologists (C.N. and W.Y.).

Lipid Identification

Lipid species were identified using high mass accuracy measurements and collision induced dissociation (CID) or higher-energy collisional dissociation (HCD) tandem MS analysis. Fragmentation patterns were compared with literature reports in conjunction with data from Lipidmaps database (www.lipidmaps.org) for identification.

2D Imaging Data Analysis

Xcalibur RAW files were converted into images using FireFly data conversion software (Prosolia, Inc. Indianapolis, IN, USA) and then uploaded into the open source imaging software package BioMAP (Novartis).

Results and Discussion

Molecular Characterization of Lymph Nodes

First, we sought to evaluate and characterize the molecular signatures of normal lymph nodes by DESI-MSI. A total of 18 normal human lymph node samples were imaged using DESI-MSI in the negative ion mode. The mass spectra obtained presented a rich diversity of molecular ions,

including small metabolites and various lipid species such as FA, SL, GL, and GP. Figure 1a shows a representative mass spectrum of normal lymph node in the range from *m/z* 100 to 1000. As observed, PI (18:0/20:4), commonly detected at *m/z* 885.551 by DESI-MSI from biological tissues, presented the highest relative abundance within all lymph node samples analyzed. In mass range from *m/z* 500 to 1000, other abundant peaks were tentatively assigned as Cer, PE, DG, PG, and PS, using high mass accuracy and tandem MS analyses. In the mass range from *m/z* 200 to 400, rich FA peaks with various lengths and unsaturation levels of carbon chains were detected, such as FA (16:1), FA (18:2), FA (20:5), FA (22:5), and FA (26:2). In the mass range from *m/z* 100 to 200, small metabolites, such as ascorbic acid (*m/z* 175.025), glutamate (*m/z* 146.047), and glutamine (*m/z* 145.062) were detected.

DESI-MSI experiments were conducted to evaluate the distribution of molecular ions in lymph node tissues. Figure 1b displays 13 representative ion images obtained for a normal lymph node tissue sample, showing a homogenous distribution of these molecular ions in normal lymph node. After DESI-MS imaging, the same tissue was H&E-stained and evaluated by histopathology, which confirmed that the tissue was composed of normal lymphocytes. A relatively homogenous distribution of molecular ions was consistently observed for regions with high density of lymphocytes within all the normal lymph node samples analyzed. In some tissues, lymph node capsule tissue, which is composed of dense irregular connective tissue surrounding lymph node cells, was also identified. The capsule tissue presented characteristic mass spectra with high abundance of TG species, detected as Cl adducts in the negative ion mode, when compared with lymphocytes (Supplementary Figure S1).

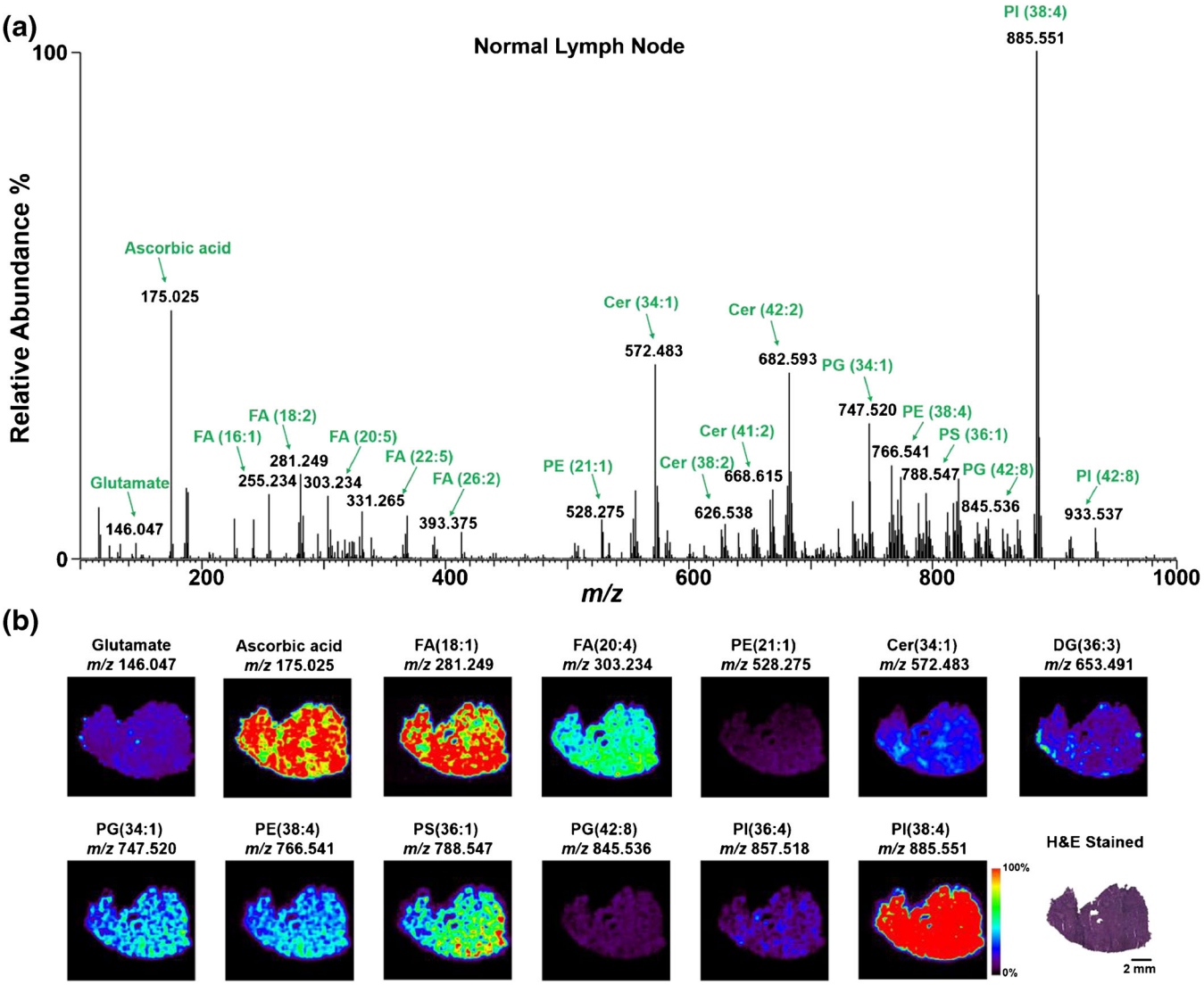

Figure 1. DESI-MS imaging of normal human lymph node tissue. (**a**) Negative-ion mode DESI-MS mass spectra obtained from normal lymph nodes with tentative attribution of selected molecular ions in green. The lipid profile is highly representative of normal lymph node tissue. (**b**) Selected DESI-MS ion images of the normal lymph node tissue including an optical image of the H&E-stained tissue section

Imaging of Metastatic Thyroid Cancer in Lymph Nodes

Papillary thyroid carcinoma is the most common form of thyroid cancer, accounting for about 80% of all thyroid cancers. Cervical metastasis, when cancer cells spread from the primary tumor to the sentinel lymph nodes in the neck, occurs in 50% of small papillary carcinomas and in more than 75% of the larger papillary carcinomas [26, 27]. Here, we used DESI-MSI to investigate the molecular profiles and distribution of eight samples of lymph nodes containing metastatic thyroid cancer. Figure 2a displays representative 2D ion images from a lymph node sample with papillary thyroid carcinoma metastasis

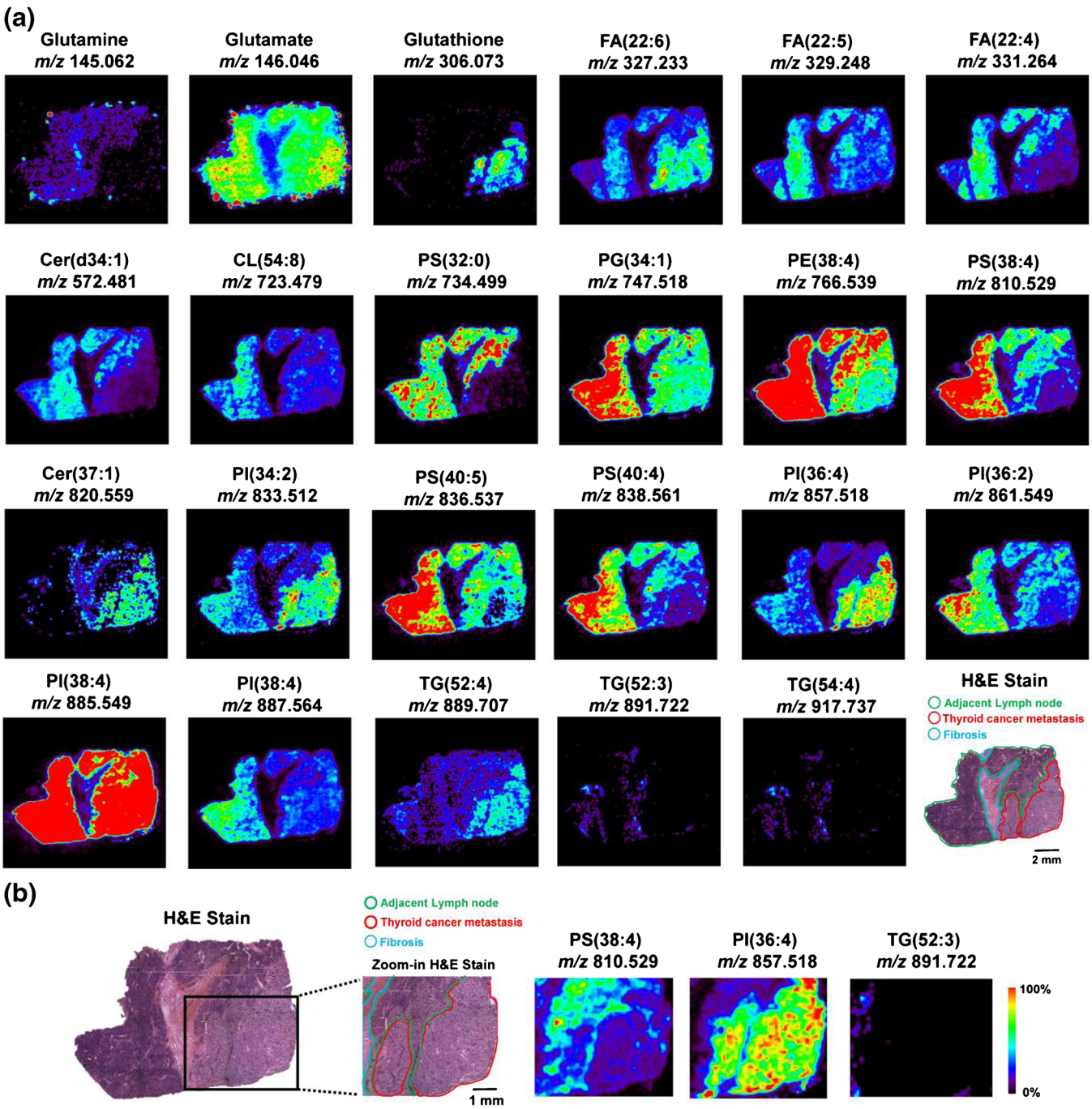

Figure 2. DESI-MS imaging of human metastatic thyroid cancer in lymph node tissue. (**a**) Twenty-three DESI-MS ion images of representative molecular ions including species identified as small metabolites, FA, and phospholipids, with distinct distribution in regions of normal lymph node, fibrosis, and metastatic thyroid cancer. An optical image of the annotated H&E-stained tissue section is also shown. (**b**) A higher magnification view of a region containing the three tissue types, highlighting the unequivocal spatial correlation of histologic features and specific molecular ions identified as PS (38:4) *m/z* 810.529, PI (36:4) *m/z* 857.518 and TG (*m/z* 891.722), is shown

analyzed by DESI-MSI. Pathologic evaluation of the H&E-stained tissue section identified regions of metastatic cancer (marked in red), adjacent normal lymph node region (marked in green), as well as fibrotic tissue (marked in blue) within the tissue sample. Distinct regions of cancer and normal lymph node tissues can be clearly visualized and discriminated in the 2D images of selected molecular ions. For example, glutamine (*m/z* 145.062) was primarily detected in the adjacent lymph node region, whereas glutathione (*m/z* 306.073) was observed almost exclusively in the cancer region. Similarly, other lipids, such as FA (22:4), Cer (34:1), PS (32:0), PG (34:1), PE (38:4), PS (38:4), PS (40:5), PS (40:4), and PI (36:2) showed higher abundances within the adjacent lymph node region in comparison to the cancer region. Conversely, other species, such as FA (327.233), PI (34:2), PI (36:4), and TG (52:4) displayed higher abundance within the cancer region than in the adjacent lymph node region. Figure 2b shows a higher magnification view of a region containing the three tissue types, highlighting the unequivocal spatial correlation of histologic features and specific molecular ions. Few molecular ions, such as glutamate (*m/z* 146.046), and PI (38:4) (*m/z* 885.551), presented similar relative abundances and even distribution in both cancerous and adjacent lymph node regions. TG species such as TG (52:3) (*m/z* 891.722) and TG (54:4) (*m/z* 917.737) were found at higher abundance in the fibrosis tissue region than in the lymph node or metastatic thyroid tumor tissue regions, similar to what was observed for lymph node capsule tissue within normal lymph node samples. Thus, the 2D ion images shown here demonstrate the ability of DESI-MSI to distinguish fibrosis, adjacent normal lymph node, and metastatic thyroid cancer based on the detection of distinct molecular profiles. Similar trends in ion abundances were observed for most of the other tissue samples presenting a mixture of metastatic papillary thyroid cancer and adjacent normal lymph node regions, although inconsistencies were seen for a few ions, such as glutathione (Supplementary Figure S2).

Changes in molecular profiles observed in adjacent lymph node and metastatic thyroid cancers were further evaluated by careful comparison of mass spectra for two interesting *m/z* regions found, *m/z* 650 to *m/z* 690, and *m/z* 805 to *m/z* 870 (Supplementary Figure S3 and Figure 3, respectively). Comparisons of the lipid alterations were performed within the same tissue section. As shown in Figure 3, PS, PG, and PI with different unsaturation levels were found in this mass range for both adjacent and cancerous lymph node. Changes in fatty acid unsaturation levels within a specific length of carbon chain of GP were observed. For example, in adjacent lymph node region, the abundance of PI (36:2) (*m/z* 861.550), which presents 36 carbons and two double bonds in the fatty acid chains, was slightly higher than that of PI (36:4) (*m/z* 857.518), which presents four double bonds in the fatty acid chains (Figure 3a). However, the pattern for these two ions was drastically different in the papillary thyroid cancer metastatic region (Figure 3b), showing a lower relative abundance of PI (36:2) (*m/z* 861.550)

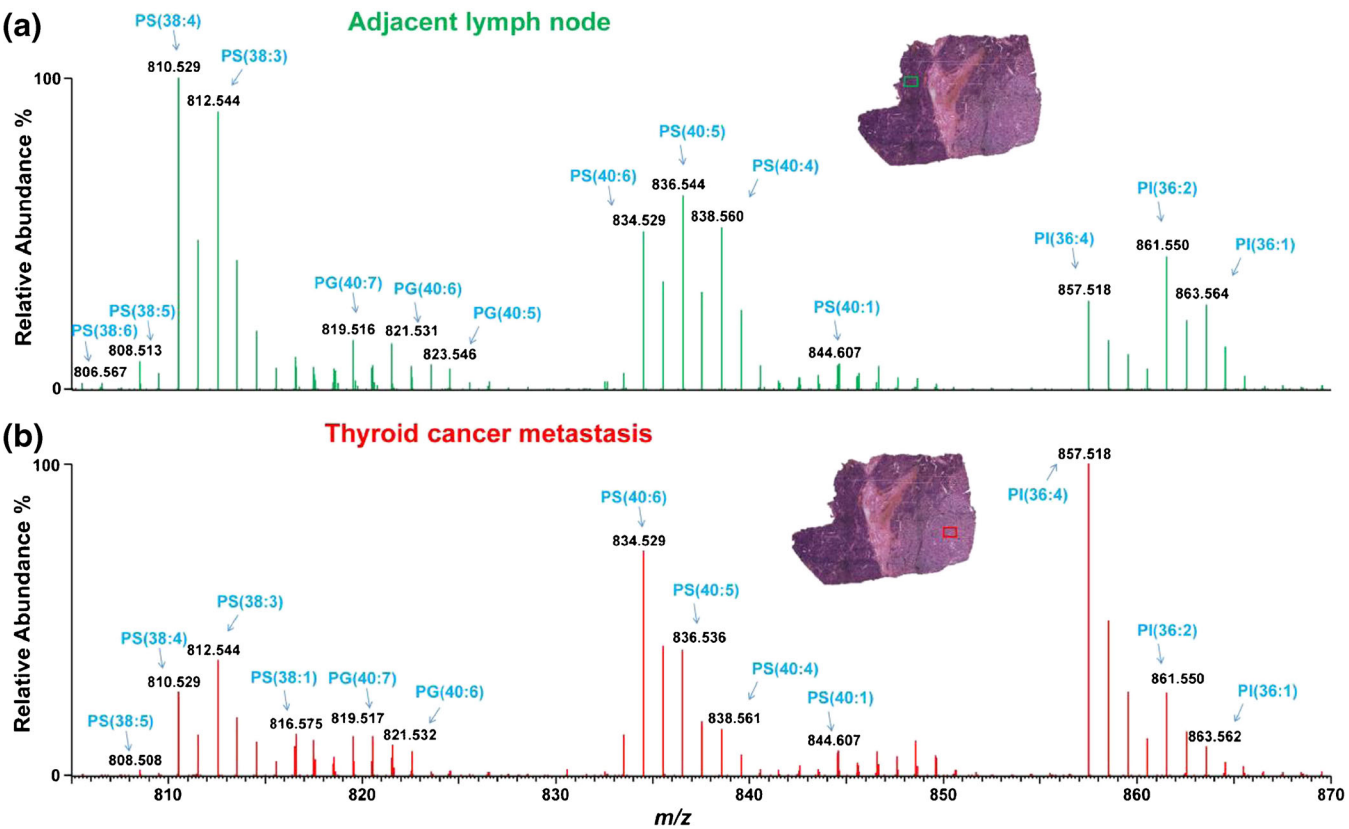

Figure 3. Representative DESI mass spectra in the mass range from *m/z* 805 to 870 extracted from (**a**) adjacent normal lymph node tissue region, and (**b**) metastatic thyroid cancer tissue region of the same sample

compared with the more unsaturated PI (36:4) (*m/z* 857.518). Similar changes were observed in the range from *m/z* 909 to 915 (Supplementary Figure S4) for PI species containing 40 carbons, PI (40:6) (*m/z* 909.550), PI (40:5) (*m/z* 911.565), and PI (40:4) (*m/z* 913.580), showing higher abundance of GPs with higher level of unsaturation in papillary thyroid cancer metastatic region compared with adjacent lymph node regions. For PS lipids, higher abundance of species with higher level of unsaturation was also observed in papillary thyroid cancer metastatic regions compared with adjacent lymph node regions for PS containing 40 carbons, PS (40:6) (*m/z* 834.529), PS (40:5) (*m/z* 836.544), and PS (40:4) (*m/z* 838.560), whereas

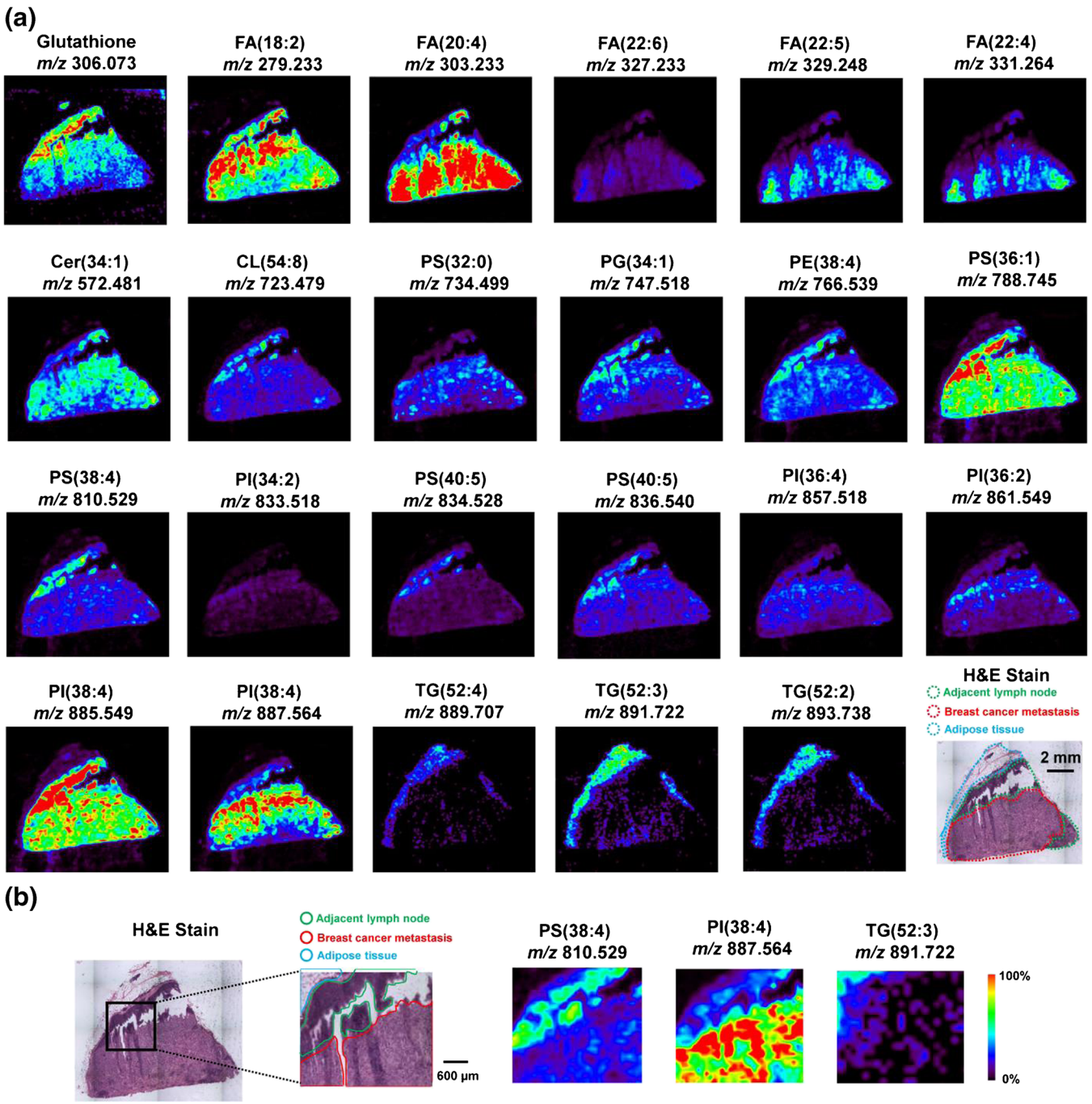

Figure 4. DESI-MS imaging of human metastatic breast cancer in lymph node tissue. (**a**) Twenty-three DESI-MS ion images of representative molecular ions including species identified as small metabolites, FA, and phospholipids, with distinct distribution in regions of normal lymph node, adipose tissue, and metastatic breast cancer. An optical image of the annotated H&E-stained tissue section is also shown. (**b**) A higher magnification view of a region containing the three tissue types, highlighting the unequivocal spatial correlation of histologic features and specific molecular ions identified as distribution of PS (38:4) *m/z* 810.529, PI (36:4) *m/z* 887.564, and TG (52:3) (*m/z* 891.722), is also shown

the trends for shorter carbon chains, PS (38:6) (*m/z* 806.567) and PS (38:5) (*m/z* 808.513) was reversed. In addition, a series of ceramides detected in the range from *m/z* 650 to 685 (Supplementary Figure S3) also has lower abundance of unsaturated lipids. Thus, alterations in the ratio of the relative abundances of two lipid species with the same fatty acid carbon chain number but different unsaturation levels have the potential to allow for differentiation between normal lymph node tissue and metastatic thyroid tumors by DESI-MSI.

Imaging of Metastatic Breast Cancer in Lymph Nodes

Nodal evaluation for invasive breast cancer is required for proper staging and helps guide adjuvant therapy [28]. A total of 16 human sentinel lymph nodes with metastatic breast cancer were analyzed to evaluate whether DESI-MSI allows discrimination of metastatic breast cancer in lymph node tissue. Figure 4 shows selected ion images of different molecular ions for a representative sample of metastatic breast cancer in lymph node. Three patterns in spatial distributions of molecular ions were observed, which strongly correlated with regions of adipose tissue (marked in blue), adjacent lymph node (marked in green), and metastatic breast cancer (marked in red), as determined by pathologic evaluation of the same tissue section after H&E staining. As observed in ion images presented in Figure 4, adipose tissue region presented higher relative abundances of TG lipids, which can be clearly seen in the 2D ion images of TG (52:4), TG (52:3), and TG(52:2). Adjacent lymph node region presented high relative abundances of PS(40:5), PS(38:4), PE(38:4), and CL(54:8) compared with metastatic breast cancer regions, which corroborates with that observed in thyroid cancer lymph node metastasis. Other lipids including PI(38:4) and fatty acids species such as FA(20:4) and FA(22:6) were observed in higher relative abundances in the metastatic breast cancer regions compared with adjacent tissues. Indeed, many studies have associated fatty acid synthesis and metabolism to breast cancer invasion and aggressiveness [28, 29]. Alterations in the abundance of fatty acids has been previously described in primary human breast cancer and animal models using DESI-MSI [7, 8] and MALDI-MSI [30]. High relative abundances of FA(20:4) and FA(22:6) were consistently observed in all metastatic breast cancer regions of the lymph node samples analyzed.

Few ions detected in sentinel lymph node breast cancer metastasis showed inverse distribution patterns compared with the ion image patterns for thyroid metastasis (Figure 2). For example, glutathione (*m/z* 306.073), which was almost exclusively detected in cancer region of lymph node thyroid metastasis, displayed higher abundance in adjacent lymph node regions instead (marked in green over the optical image of H&E-stained tissue in Figure 4a). Glutathione is a natural tripeptide that plays important roles in various cellular processes, including antioxidation, cell differentiation, proliferation, and apoptosis. Altered levels of glutathione have been reported in various types of tumors [31]. Interestingly, glutathione

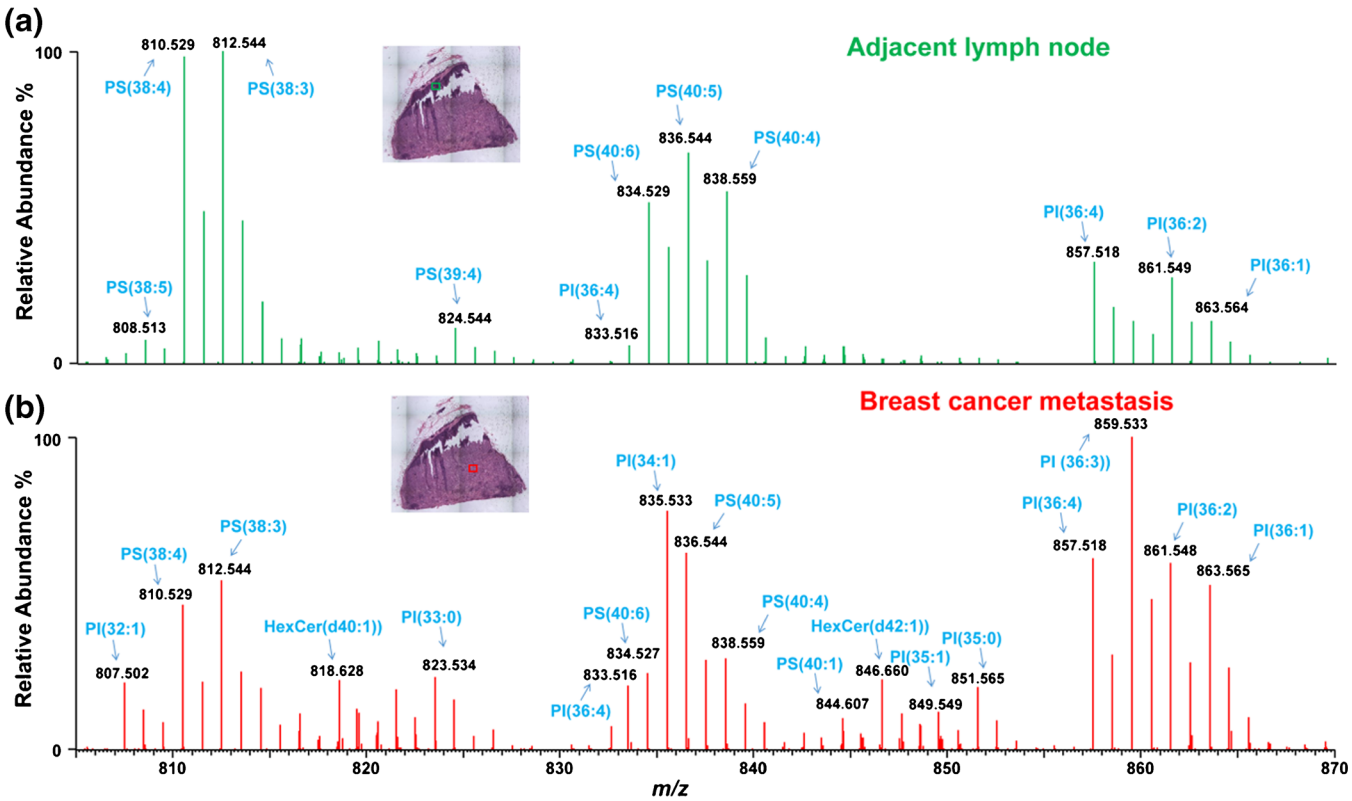

Figure 5. Representative DESI mass spectra in the mass range from *m/z* 805 to 870 extracted from (**a**) adjacent normal lymph node tissue region, and (**b**) metastatic breast cancer tissue region of the same sample

metabolism is able to play both protective and pathogenic roles, and have been specifically linked to resistance to chemotherapy [32]. Thus, the changes in relative abundances of glutathione observed by DESI-MSI may be patient-dependent rather disease-specific, and should be further evaluated. Other molecules detected, such as FA (22:4) (*m*/*z* 331.264), Cer (d34:1) (*m*/*z* 572.481), PS (34:1) (*m*/*z* 734.499), and PI (38:4) (*m*/*z* 887.564), also presented opposite distribution patterns with that of lymph node thyroid metastasis when comparing metastatic and adjacent lymph node tissues.

Detailed investigation of changes in relative abundances of specific lipid species within narrow *m*/*z* ranges in lymph node breast cancer metastasis was performed. As seen in Figure 5 (*m*/*z* 805 to 870), the relative abundance of PI species containing 36 carbons with higher degree of unsaturation was decreased in comparison to more saturated species when comparing metastatic breast cancer and adjacent normal lymph node tissues, as clearly observed for PI (36:4) (*m*/*z* 857.518) and PI (36:3) (*m*/*z* 859.533). Increases in the relative abundance of PI lipids with shorter carbon chains, such as PI (32:1) (*m*/*z* 807.502), PI (33:0) (*m*/*z* 823.534), PI (35:1) (*m*/*z* 849.549), and PI (35:0) (*m*/*z* 851.565), were seen in the mass spectra of metastatic breast cancer compared with adjacent lymph node. Higher relative abundances of cardiolipins (CL) were seen in the mass range (*m*/*z* 670 to 705) in lymph node breast cancer metastasis, which were not detected in the adjacent lymph node tissue (Supplementary Figure S5). However, PA species, including PA (34:2) (*m*/*z* 671.466), PA (34:1) (*m*/*z* 673.481), PA (36:4) (*m*/*z* 695.466), and PA (36:1) (*m*/*z* 699.496), were present at a lower relative abundance in metastatic breast cancer tissues compared with adjacent normal lymph node (Supplementary Figure S5). Similar trends were observed for the other metastatic lymph node samples analyzed, although a larger sample cohort and statistical evaluation are needed to define significant markers.

Conclusions

We have shown that DESI-MSI can be used to detect and visualize human metastatic thyroid and breast cancer tissues within lymph nodes based on alterations in the abundances of lipids and metabolites. 2D DESI-MS images of specific molecular ions enable clear discrimination of metastatic cancer from other histologic features of the tissue sections, including adjacent normal lymph node tissue and other supportive tissues such as fibrosis and adipose tissues. Through comparison of ion images with pathologic evaluation, changes in relative abundances of specific molecular ions were clearly observed, leading to the inference that some ions could serve as diagnostic markers for detection of thyroid and breast cancer metastasis in lymph node tissues.

Comparison of the mass spectra profiles extracted from regions with a predominant histologic feature in the ion images allowed evaluation of molecular changes associated with metastatic breast, thyroid, and normal lymph node tissues. Distributions of small metabolites, such as glutamine, showed opposite spatial distributions in cancer metastasis and the adjacent normal lymph nodes, respectively. Distribution of glutathione was also distinct in different tissue regions, although inconsistencies across different patients were observed. Several other lipid species, including CL, PI, PS, and Cer, allowed discrimination of metastatic cancer and adjacent normal tissues. Similarly, molecular distributions of FA and GP showed the potential to distinguish between breast cancer metastasis and adjacent normal lymph node tissue. In particular, arachidonic acid, FA(20:4), and docosapentaenoic acid, FA(22:5), showed high relative intensities in the metastatic breast cancer regions compared with adjacent normal lymph node and adipose tissues.

Comparisons of normal lymph node and thyroid tumor tissue spectra showed alterations in fatty acyl unsaturation levels for PS, PG, and PI lipid species in thyroid cancer metastasis. GP species with longer FA carbon chains presented higher levels of unsaturation in papillary carcinoma regions of the tissue compared with normal lymph node regions, whereas shorter carbon chains had reduced levels of unsaturation within the tumor regions. Conversely, while breast cancer metastasis showed differences in unsaturation levels between tumor and normal tissue as well, these tissues exhibited the opposite trend, with longer carbon chains with low levels on unsaturation and short carbon chains with high levels of unsaturation being more abundant in the breast cancer tissue than in the adjacent normal lymph node.

In summary, our results demonstrate the potential of DESI-MSI for lymph node diagnosis to aid in the staging of human thyroid and breast cancers. This is the first example of the use of DESI-MSI for investigation of the metabolic signatures of breast and thyroid cancer metastasis. As ambient ionization MS technologies have been increasingly explored for intraoperative cancer diagnosis, we expect DESI-MSI and other ambient ionization MS techniques to be used for cancer staging through lymph node analysis. Note that while this study demonstrates the use of DESI-MS for tissue section imaging, the time needed for sectioning (~15 min) and MS imaging (~30 min) could limit its use for rapid lymph node evaluation. Thus, we are exploring the use of DESI-MSI for lymph node analysis using alternative sample preparation approaches such as touch imprint biopsies, which are routinely used for rapid intraoperative lymph node analysis by cytopathology [34]. Further, we envision DESI-MS to be used to assess specific tissue regions with ambiguous lymph node diagnosis by histopathology, at a faster operating rate, which may improve throughput and accuracy in cancer staging in clinical practice. Although consistent trends in abundances of specific molecular ions were observed for the 42 tissue samples analyzed, further experiments with a larger sample cohort will be pursued to confirm these findings. Importantly, statistical analysis will also be pursued to determine metabolic markers that significantly characterize metastatic breast and thyroid tissues, and to develop statistical classifiers for rapid tissue diagnosis in order to validate the usefulness of DESI-MSI as an accurate technology for cancer staging.

Acknowledgments

The authors acknowledge support for this work by the NIH/NCI (grant R00CA190783). Tissue samples were provided by the Cooperative Human Tissue Network, which is funded by the NCI.

References

1. Heeren, R.M.A.: Getting the picture: the coming of age of imaging MS. Int. J. Mass Spectrom. **377**, 672–680 (2015)
2. Ifa, D.R., Eberlin, L.S.: Ambient ionization mass spectrometry for cancer diagnosis and surgical margin evaluation. Clin. Chem. **62**, 111–123 (2016)
3. Eberlin, L.S., Norton, I., Orringer, D., Dunn, I.F., Liu, X., Ide, J.L., Jarmusch, A.K., Ligon, K.L., Jolesz, F.A., Golby, A.J., Santagata, S., Agar, N.Y., Cooks, R.G.: Ambient mass spectrometry for the intraoperative molecular diagnosis of human brain tumors. Proc. Natl. Acad. Sci. U. S. A. **110**, 1611–1616 (2013)
4. Kerian, K.S., Jarmusch, A.K., Pirro, V., Koch, M.O., Masterson, T.A., Cheng, L., Cooks, R.G.: Differentiation of prostate cancer from normal tissue in radical prostatectomy specimens by desorption electrospray ionization and touch spray ionization mass spectrometry. Analyst **140**, 1090–1098 (2015)
5. Eberlin, L.S., Tibshirani, R.J., Zhang, J.L., Longacre, T.A., Berry, G.J., Bingham, D.B., Norton, J.A., Zare, R.N., Poultsides, G.A.: Molecular assessment of surgical-resection margins of gastric cancer by mass-spectrometric imaging. Proc. Natl. Acad. Sci. U. S. A. **111**, 2436–2441 (2014)
6. Janfelt, C., Wellner, N., Hansen, H.S., Hansen, S.H.: Displaced dual-mode imaging with desorption electrospray ionization for simultaneous mass spectrometry imaging in both polarities and with several scan modes. J. Mass Spectrom. **48**, 361–366 (2013)
7. Calligaris, D., Caragacianu, D., Liu, X.H., Norton, I., Thompson, C.J., Richardson, A.L., Golshan, M., Easterling, M.L., Santagata, S., Dillon, D.A., Jolesz, F.A., Agar, N.Y.R.: Application of desorption electrospray ionization mass spectrometry imaging in breast cancer margin analysis. Proc. Natl. Acad. Sci. U. S. A. **111**, 15184–15189 (2014)
8. Guenther, S., Muirhead, L.J., Speller, A.V., Golf, O., Strittmatter, N., Ramakrishnan, R., Goldin, R.D., Jones, E., Veselkov, K., Nicholson, J., Darzi, A., Takats, Z.: Spatially resolved metabolic phenotyping of breast cancer by desorption electrospray ionization mass spectrometry. Cancer Res. **75**, 1828–1837 (2015)
9. Walsh, C.M., Reschke, B.R., Fortney, J., Piktel, D., Razunguzwa, T.T., Powell, M.J., Gibson, L.F.: A novel laser ablation electrospray ionization mass spectrometry (LAESI-MS) platform for biomarker discovery in cancer cells. Cancer Res. **72**, 4793–4793 (2012).
10. Golf, O., Strittmatter, N., Karancsi, T., Pringle, S.D., Speller, A.V., Mroz, A., Kinross, J.M., Abbassi-Ghadi, N., Jones, E.A., Takats, Z.: Rapid evaporative ionization mass spectrometry imaging platform for direct mapping from bulk tissue and bacterial growth media. Anal. Chem. **87**, 2527–2534 (2015)
11. Laskin, J., Heath, B.S., Roach, P.J., Cazares, L., Semmes, O.J.: Tissue imaging using nanospray desorption electrospray ionization mass spectrometry. Anal. Chem. **84**, 141–148 (2012)
12. Hsu, C.C., Dorrestein, P.C.: Visualizing life with ambient mass spectrometry. Curr. Opin. Biotechnol. **31**, 24–34 (2015)
13. Laskin, J., Lanekoff, I.: Ambient mass spectrometry imaging using direct liquid extraction techniques. Anal. Chem. **88**, 52–73 (2016)
14. Liu, L.C., Lang, J.E., Lu, Y., Roe, D., Hwang, S.E., Ewing, C.A., Esserman, L.J., Morita, E., Treseler, P., Leong, S.P.: Intraoperative frozen section analysis of sentinel lymph nodes in breast cancer patients: a meta-analysis and single-institution experience. Cancer **117**, 250–258 (2011)
15. Tsujimoto, M., Nakabayashi, K., Yoshidome, K., Kaneko, T., Iwase, T., Akiyama, F., Kato, Y., Tsuda, H., Ueda, S., Sato, K., Tamaki, Y., Noguchi, S., Kataoka, T.R., Nakajima, H., Komoike, Y., Inaji, H., Tsugawa, K., Suzuki, K., Nakamura, S., Daitoh, M., Otomo, Y., Matsuura, N.: One-step nucleic acid amplification for intraoperative detection of lymph node metastasis in breast cancer patients. Clin. Cancer Res. **13**, 4807–4816 (2007)
16. Albertini, J.J., Cruse, C.W., Rapaport, D., Wells, K., Ross, M., DeConti, R., Berman, C.G., Jared, K., Messina, J., Lyman, G., Glass, F., Fenske, N., Reintgen, D.S.: Intraoperative radio-lympho-scintigraphy improves sentinel lymph node identification for patients with melanoma. Ann. Surg. **223**, 217–224 (1996)
17. Sattlecker, M., Bessant, C., Smith, J., Stone, N.: Investigation of support vector machines and Raman spectroscopy for lymph node diagnostics. Analyst **135**, 895–901 (2010)
18. Grigsby, P.W., Siegel, B.A., Dehdashti, F.: Lymph node staging by positron emission tomography in patients with carcinoma of the cervix. J. Clin. Oncol. **19**, 3745–3749 (2001)
19. Yasufuku, K., Nakajima, T., Motoori, K., Sekine, Y., Shibuya, K., Hiroshima, K., Fujisawa, T.: Comparison of endobronchial ultrasound, positron emission tomography, and CT for lymph node staging of lung cancer. Chest **130**, 710–718 (2006)
20. Pei, H., Zhu, H., Zeng, S., Li, Y., Yang, H., Shen, L., Chen, J., Zeng, L., Fan, J., Li, X., Gong, Y., Shen, H.: Proteome analysis and tissue microarray for profiling protein markers associated with lymph node metastasis in colorectal cancer. J. Proteome Res. **6**, 2495–2501 (2007)
21. Fumagalli, D., Gavin, P.G., Taniyama, Y., Kim, S.I., Choi, H.J., Paik, S., Pogue-Geile, K.L.: A rapid, sensitive, reproducible and cost-effective method for mutation profiling of colon cancer and metastatic lymph nodes. BMC Cancer **10**, 101 (2010)
22. Pang, J., Liu, W.P., Liu, X.P., Li, L.Y., Fang, Y.Q., Sun, Q.P., Liu, S.J., Li, M.T., Su, Z.L., Gao, X.: Profiling protein markers associated with lymph node metastasis in prostate cancer by DIGE-based proteomics analysis. J. Proteome Res. **9**, 216–226 (2010)
23. Barekati, Z., Radpour, R., Lu, Q., Bitzer, J., Zheng, H., Toniolo, P., Lenner, P., Zhong, X.Y.: Methylation signature of lymph node metastases in breast cancer patients. BMC Cancer **12**, 244 (2012)
24. Abbassi-Ghadi, N., Veselkov, K., Kumar, S., Huang, J., Jones, E., Strittmatter, N., Kudo, H., Goldin, R., Takats, Z., Hanna, G.B.: Discrimination of lymph node metastases using desorption electrospray ionisation-mass spectrometry imaging. Chem. Commun. **50**, 3661–3664 (2014)
25. Abbassi-Ghadi, N., Golf, O., Kumar, S., Antonowicz, S., McKenzie, J.S., Huang, J., Strittmatter, N., Kudo, H., Jones, E.A., Veselkov, K., Goldin, R., Takats, Z., Hanna, G.B.: Imaging of esophageal lymph node metastases by desorption electrospray ionization mass spectrometry. Cancer Res. **19**, 5647–5656 (2016)
26. Randolph, G.W., Duh, Q.Y., Heller, K.S., LiVolsi, V.A., Mandel, S.J., Steward, D.L., Tufano, R.P., Tuttle, R.M.: Amercan Thyroid Association Surgical, A: the prognostic significance of nodal metastases from papillary thyroid carcinoma can be stratified based on the size and number of metastatic lymph nodes, as well as the presence of extranodal extension. Thyroid **22**, 1144–1152 (2012)
27. Lee, J., Song, Y., Soh, E.Y.: Prognostic significance of the number of metastatic lymph nodes to stratify the risk of recurrence. World J. Surg. **38**, 858–862 (2014)
28. Nomura, D.K., Long, J.Z., Niessen, S., Hoover, H.S., Ng, S.W., Cravatt, B.F.: Monoacylglycerol lipase regulates a fatty acid network that promotes cancer pathogenesis. Cell **140**, 49–61 (2010)
29. Alo, P.L., Visca, P., Marci, A., Mangoni, A., Botti, C., DiTondo, U.: Expression of fatty acid synthase (FAS) as a predictor of recurrence in stage I breast carcinoma patients. Cancer **77**, 474–482 (1996)
30. Mascini, N.E., Cheng, M.L., Jiang, L., Rizwan, A., Podmore, H., Bhandari, D.R., Rompp, A., Glunde, K., Heeren, R.M.A.: Mass spectrometry imaging of the hypoxia marker pimonidazole in a breast tumor model. Anal. Chem. **88**, 3107–3114 (2016)
31. Balendiran, G.K., Dabur, R., Fraser, D.: The role of glutathione in cancer. Cell Biochem. Funct. **22**, 343–352 (2004)
32. Traverso, N., Ricciarelli, R., Nitti, M., Marengo, B., Furfaro, A.L., Pronzato, M.A., Marinari, U.M., Domenicotti, C.: Role of glutathione in cancer progression and chemoresistance. Oxidative Med. Cellular Longevity. (2013)
33. van Diest, P.J., Torrenga, H., Borgstein, P.J., Pijpers, R., Bleichrodt, R.P., Rahusen, F.D., Meijer, S.: Reliability of intraoperative frozen section and imprint cytological investigation of sentinel lymph nodes in breast cancer. Histopathology **35**, 14–18 (1999)
34. Turner, R.R., Hansen, N.M., Stern, S.L., Giuliano, A.E.: Intraoperative examination of the sentinel lymph node for breast carcinoma staging. Am. J. Clin. Pathol. **112**, 627–634 (1999)